

---

# The Role of ImageNet Classes in Fréchet Inception Distance

---

**Tuomas Kynkäänniemi**

Aalto University

tuomas.kynkaanniemi@aalto.fi

**Tero Karras**

NVIDIA

tkarras@nvidia.com

**Miika Aittala**

NVIDIA

maittala@nvidia.com

**Timo Aila**

NVIDIA

taila@nvidia.com

**Jaakko Lehtinen**

Aalto University

NVIDIA

jlehtinen@nvidia.com

## Abstract

Fréchet Inception Distance (FID) is a metric for quantifying the distance between two distributions of images. Given its status as a standard yardstick for ranking models in data-driven generative modeling research, it seems important that the distance is computed from general, “vision-related” features. But is it? We observe that FID is essentially a distance between sets of ImageNet class probabilities. We trace the reason to the fact that the standard feature space, the penultimate “pre-logit” layer of a particular Inception-V3 classifier network, is only one affine transform away from the logits, i.e., ImageNet classes, and thus, the features are necessarily highly specialized to them. This has unintuitive consequences for the metric’s sensitivity. For example, when evaluating a model for human faces, we observe that, on average, FID is actually very insensitive to the facial region, and that the probabilities of classes like “bow tie” or “seat belt” play a much larger role. Further, we show that FID can be significantly reduced — without actually improving the quality of results — by an attack that first generates a slightly larger set of candidates, and then chooses a subset that happens to match the histogram of such “fringe features” in the real data. We then demonstrate that this observation has practical relevance in case of ImageNet pre-training of GANs, where a part of the observed FID improvement turns out not to be real. Our results suggest caution against over-interpreting FID improvements, and underline the need for distribution metrics that are more perceptually uniform.

## 1 Introduction

Generative modeling has been an extremely active research topic in recent years. Many prominent model types, such as generative adversarial networks (GAN) [14], variational autoencoders (VAE) [27], autoregressive models [36, 37], flow models [10, 26] and diffusion models [17, 52, 53] have seen significant improvement. Additionally, these models have been applied to a rich set of downstream tasks, such as realistic image synthesis [4, 12, 21–24, 45], unsupervised domain translation [6, 25, 62], image super resolution [2, 30, 46], image editing [18, 38, 39] and generating images based on a text prompt [35, 44].

Given the large number of applications and rapid development of the models, designing evaluation metrics for benchmarking their performance is an increasingly important topic. It is crucial to be able to reliably rank models and pinpoint improvements caused by specific changes in the models or training setups. Ideally, a generative model should produce samples that are indistinguishable from

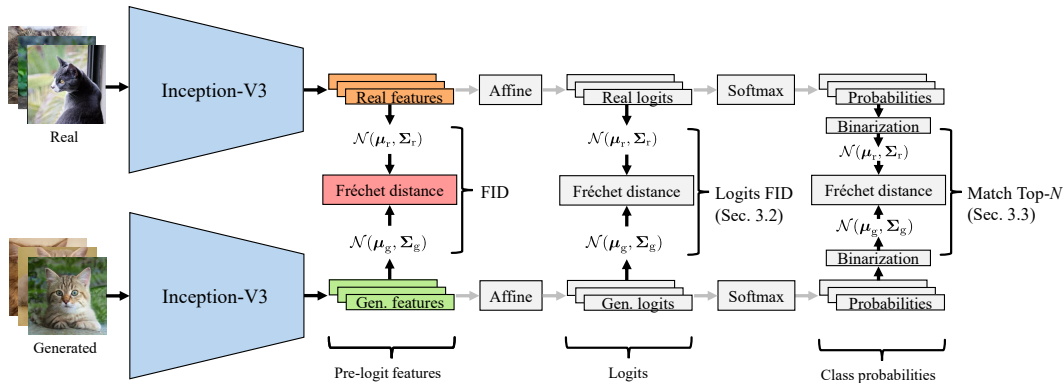


Figure 1: Overview of the Fréchet Inception Distance (FID) [16]. First, the real and generated images are separately passed through a pre-trained classifier network, typically the Inception-V3 [54], to produce two sets of feature vectors. Then, both distributions of features are approximated with multivariate Gaussians, and FID is defined as the Fréchet distance between the two Gaussians. In Section 3, we will compute alternative FIDs in the feature spaces of logits and class probabilities, instead of the usual pre-logit space.

the training set, while covering all of its variation. To quantitatively measure these aspects, numerous metrics have been proposed, including Inception Score (IS) [48], Fréchet Inception Distance (FID) [16], Kernel Inception Distance (KID) [3], and Precision/Recall [29, 34, 47]. As an alternative to these automatic metrics, a human-in-the-loop evaluation of model quality has been described [61]. Among these metrics, FID continues to be the primary tool for quantifying progress. Our main message is that singular focus on FID may lead to false conclusions, and our results demonstrate some of its unintuitive behavior.

The key idea in FID [16] is to separately embed real and generated images to a *vision-relevant feature space*, and compute a distance between the two distributions, as illustrated in Figure 1. In practice, the feature space is the penultimate layer (*pool3*, 2048 features) of an ImageNet [8] pre-trained Inception-V3 classifier network [54], and the distance is computed as follows. The distributions of real and generated embeddings are separately approximated by multivariate Gaussians, and their alignment is quantified using the Fréchet (equivalently, the 2-Wasserstein or earth mover’s) distance [11]

$$\text{FID}(\mu_r, \Sigma_r, \mu_g, \Sigma_g) = \|\mu_r - \mu_g\|_2^2 + \text{Tr}(\Sigma_r + \Sigma_g - 2(\Sigma_r \Sigma_g)^{\frac{1}{2}}), \quad (1)$$

where  $(\mu_r, \Sigma_r)$ , and  $(\mu_g, \Sigma_g)$  denote the sample mean and covariance of the embeddings of the real and generated data, respectively, and  $\text{Tr}(\cdot)$  indicates the matrix trace. By measuring the distance between the real and generated embeddings, FID is a clear improvement over IS [48], which ignores the real data altogether. FID has been found to correlate reasonably well with human judgments of the fidelity of generated images [16, 32, 58]; it is also conceptually simple and fast to compute. However, it conflates the resemblance to real data and the amount of variation to a single value [29, 47], and its numerical value is significantly affected by various details, including the sample count [3, 7], the architecture (and instance) of the feature network, and even low-level image processing details [40]. Following standard practice, we compute FID against the training set, using 50k randomly chosen real and generated images and the official TensorFlow version of Inception-V3.<sup>1</sup>

The implicit assumption in FID is that the feature space embeddings have general perceptual relevance. If this were the case, a certain improvement in FID would indicate a corresponding perceptual improvement in the images. While feature spaces with approximately this property have been identified [60], there are several reasons why we doubt that FID’s feature space behaves like this. *First*, the known perceptual feature spaces have very high dimensionality ( $\sim 6M$ ), partially because they consider the spatial position of features as well. Unfortunately, there may be a contradiction between perceptual relevance and distribution statistics. It is not clear how much perceptual relevance small feature spaces (2048D for FID) can have, but it is also hard to see how distribution statistics

<sup>1</sup><http://download.tensorflow.org/models/image/imagenet/inception-2015-12-05.tgz>

could be defined and compared in very large feature spaces. *Second*, FID’s feature space is specialized to classification, where the goal is to produce accurate predictions of the Top-1 class. It is therefore allowed to be blind to any image features that fail to help with this goal. *Third*, FID’s feature space (“pre-logits”) is only one affine transformation away from the logits, from which a softmax produces the ImageNet class probabilities. This necessarily means that the feature space is highly specialized to the ImageNet classes: we observe high correlation between FIDs computed from pre-logits and logits. It can thus be argued that the features correspond directly to ImageNet classes. *Fourth*, ImageNet classifiers are known to base their decisions primarily on textures instead of shapes [13, 15]. This disagreement with human perception is inherited to FID.

Together, these properties have important practical consequences that we set out to investigate. In Section 2 we use a gradient-based visualization technique, Grad-CAM [51], to visualize what FID “looks at” in generated images, and observe that its fixation on the most prominent ImageNet classes makes it more interested in, for example, seat belts and suits, than the human faces in FFHQ [23]. It becomes clear that when a significant domain gap exists between a dataset of interest and ImageNet, many of the activations related to ImageNet class templates are rather coincidental. We call such poorly fitting templates *fringe features* or fringe classes. As matching the distribution of such fringe classes between real and generated images becomes an obvious way of manipulating FID, we examine such “attacks” in detail in Section 3. The unfortunate outcome is that FID can be significantly improved without any improvement in the generated images by selecting a subset of images that happen to match some number of fringe features with the real data.

We conclude with an example of practical relevance in Section 4, showing that not all of the FID improvement coming from ImageNet pre-training in GANs is real. Some of it comes from accidental leaking of ImageNet features, and the consequent better reproduction of ImageNet-like aspects in the real data. This causes an inconsistent evaluation between two state-of-the-art GANs, StyleGAN2 [21] and Projected FastGAN [31, 49]. The result is in line with the recent findings of Morozov et al. [33], who observe a similar reversal between FID and observed image quality of various GANs.

## 2 What does FID look at in an image?

We will now inspect to which parts of an image FID is the most sensitive to. We rely on Grad-CAM [51], which has been extensively used for visualizing the parts of an image that contribute the most to the decisions of a classifier. We want to use it similarly for visualizing which parts of one generated image contribute the most to FID. A key challenge is that FID is defined only between large sets of images (50k), not for a single image. We address this difficulty by pre-computing the required statistics for a set of 49,999 generated images, and augmenting them with the additional image of interest. We then use Grad-CAM to visualize the parts of the image that have the largest influence on FID.

We will first explain our visualization technique, followed by observations from individual images, and from aggregates of images.

### 2.1 Our visualization technique

Figure 2 gives an outline of our visualization technique. Assume we have pre-computed the mean and covariance statistics  $(\mu_r, \Sigma_r)$  and  $(\mu_g, \Sigma_g)$  for 50,000 real and 49,999 generated images, respectively. These Gaussians are treated as constants in our visualization. Now, we want to update the statistics of the generated images by adding one new image. Computing the FID from the updated statistics allows us to visualize which parts of the added image influence it the most. Given an image, we feed it through the Inception-V3 network to get activations  $A^k$  before the *pool3* layer. The spatial resolution here is  $8 \times 8$  and there are 2048 feature maps. The spatial averages of these feature maps correspond to the 2048-dimensional feature space where FID is calculated. We then update the pre-computed statistics  $(\mu_g, \Sigma_g)$  by including the features  $\mathbf{f}$  of the new sample [42]:  $(\mu'_g = \frac{N-1}{N}\mu_g + \frac{1}{N}\mathbf{f}, \Sigma'_g = \frac{N-2}{N-1}\Sigma_g + \frac{1}{N}(\mathbf{f} - \mu_g)^T(\mathbf{f} - \mu_g))$ . Here,  $N = 50,000$  is the size of the updated set. To complete the forward pass, we evaluate FID using these modified statistics.

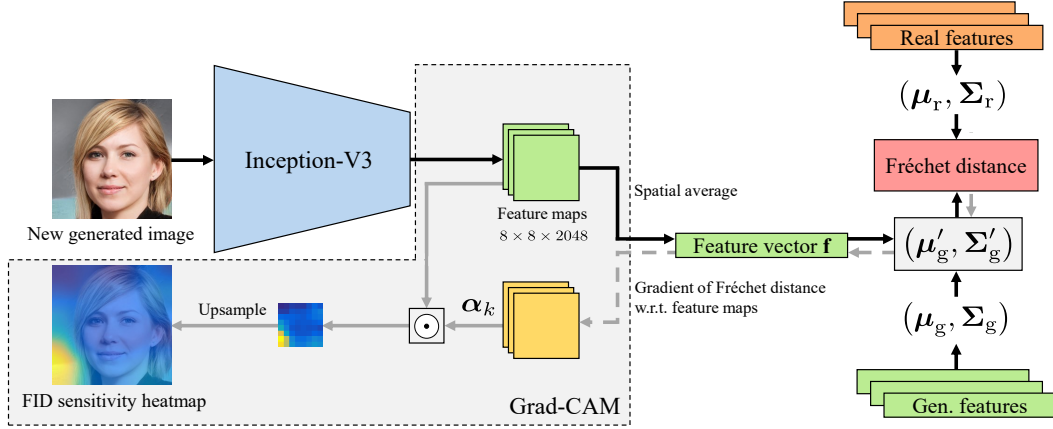


Figure 2: Visualizing which regions of an image FID is the most sensitive to. We augment the pre-computed feature statistics with a newly generated image, compute the FID, and use Grad-CAM [51] to visualize the spatial importance in low-resolution feature maps that are subsequently upsampled to match the input resolution.

In a backward pass, we first estimate the importance  $\alpha_k$  for each of the  $k$  feature maps as

$$\alpha_k = \frac{1}{8 \times 8} \sum_i \sum_j \left| \frac{\partial \text{FID}(\mu_r, \Sigma_r, \mu'_g, \Sigma'_g)}{\partial \mathbf{A}_{ij}^k} \right|^2 \quad (2)$$

Then, an  $8 \times 8$ -pixel spatial importance map is computed as a linear combination  $\sum_k \alpha_k \mathbf{A}^k$ . Note that we omit ReLU which was suggested by [51] to visualize image regions that have a positive effect in maximizing classification probabilities of a certain class. Instead, we want to see all regions for which FID is sensitive to. Additionally, we upsample the importance map using Lanczos filtering to match the dimensions of the input image and avoid aliasing. Finally, the values of the importance map are converted to a heatmap visualization.

## 2.2 Observations from individual images

Figure 3 shows overlays of Grad-CAM heatmaps of the most important regions for FID for StyleGAN2 generated images in FFHQ [23] and LSUN CAT [59]. Given that in FFHQ the goal is to generate realistic human faces, the regions FID considers most important seem rather unproductive. They are typically outside the person’s face. To better understand why this might happen, recall that ImageNet does not include a “person” or a “face” category. Instead, some other fringe features (and thus classes) are necessarily activated for each generated image. Interestingly, we observe that the heatmaps seem to correspond very well with the areas that the image’s ImageNet Top-1 class prediction would occupy. Note that these ImageNet predictions were not used when computing the heatmap; they are simply a tool for understanding what FID was focusing on. As a low FID mandates that the distributions of the most prominent fringe classes are matched between real and generated images, one has to wonder how relevant it really is to match the distributions of “seat belt” or “oboe” in this dataset. In any case, managing to perform such matching would seem to open a possible loophole in FID; we will investigate this further in Section 3.

In contrast to human faces, ImageNet does include multiple categories of cats. This helps FID to much better focus on the subject matter in LSUN CAT, although some fringe features from the image background are still getting picked up, and a very low FID would require that “washbasin”, etc. are similarly detected in real and generated images.

## 2.3 Observations from aggregates of images

Figure 4a shows the distribution of ImageNet Top-1 classifications for real and generated images in FFHQ. Typically, the predicted classes are accessories, but their presence might be correlated

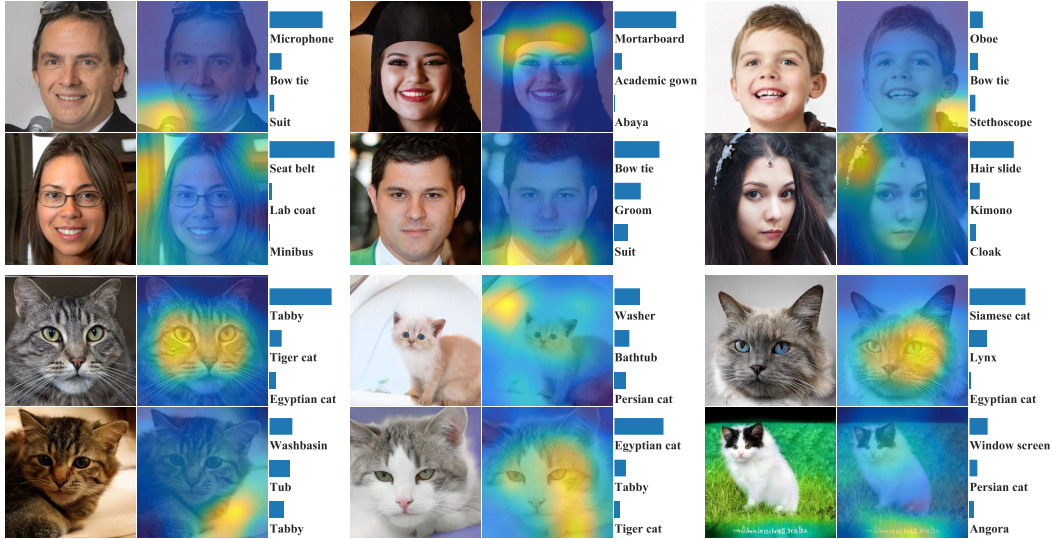


Figure 3: StyleGAN2-generated images along with heatmap visualizations of the image regions that FID considers important in FFHQ (top) and LSUN CAT (bottom). Yellow indicates regions that are more important and blue regions that are less important, i.e., modifying the content of the yellow regions affects FID most strongly. As many of the yellow areas are completely outside the intended subject, we sought an explanation from the Top-3 ImageNet class predictions for the generated image. It turns out that FID is very strongly focused on the area that corresponds to the predicted Top-1 class — whatever that may be.

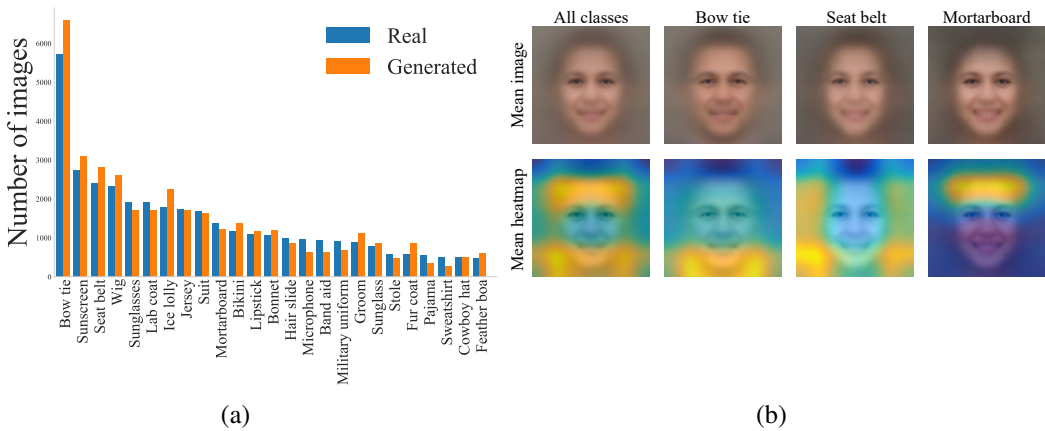


Figure 4: (a) Distribution of the ImageNet Top-1 classes, predicted by Inception-V3, for real and StyleGAN2 generated images in FFHQ. (b) Mean images and Grad-CAM heatmaps among all classes, and images classified as “bow tie”, “seat belt” and “mortarboard” categories. Strikingly, when averaging over all classes, FID is the most sensitive to ImageNet objects that are located outside the face area.

with persons in the images. In a further test, we calculated a heatmap of the average sensitivity over 50k images. Figure 4b shows average images and heatmaps for all classes, and for images that are classified to some specific class (e.g., “bow tie”). If we average over all classes, FID is the most sensitive to other areas of the image than the human face. If we compute a heatmap of the average sensitivity within a class, they highlight the regions where the corresponding ImageNet class is typically located in the images. The supplementary material provides additional single image heatmaps and average heatmaps. It also provides further validation, by selectively adding noise to regions considered either important or unimportant by the Grad-CAM visualization, that the image regions that FID is the most sensitive to are correctly highlighted by our approach.

Table 1: Results of Top-1 histogram matching. We compare the FID of randomly sampled images (FID) against ones that have been resampled to match the Top-1 histogram of the training data (FID<sup>Top-1</sup>). The numbers represent averages over five FID evaluations. Additionally, we report the corresponding numbers by replacing the Inception-V3 feature space with CLIP features (FID<sub>CLIP</sub>, FID<sub>CLIP</sub><sup>Top-1</sup>). Note that we use CLIP only when computing FID; the resampling is still done using Inception-V3. The numerical values of FID and FID<sub>CLIP</sub> are not comparable.

Dataset	FID	FID <sup>Top-1</sup>	FID <sub>CLIP</sub>	FID <sub>CLIP</sub> <sup>Top-1</sup>
FFHQ	5.63	4.91 (-12.8%)	2.90	2.86 (-1.4%)
LSUN CAT	8.35	7.37 (-11.7%)	8.95	8.83 (-1.3%)
LSUN CAR	5.75	5.17 (-10.1%)	7.76	7.73 (-0.4%)
LSUN PLACES	13.05	11.76 (-9.9%)	16.36	16.17 (-1.2%)
AFHQ-v2 DOG	10.58	9.39 (-11.2%)	4.23	4.16 (-1.7%)

In related work, Steenkiste et al. [56] found that in images with multiple salient objects, FID focuses on only one of them and hypothesized that the metric could be easily fooled by a generative model that focuses on some image statistics (e.g., generating correct number of objects) rather than content. They hypothesized that this is because Inception-V3 is trained on a single object classification.

### 3 Probing the perceptual null space in FID

Our findings with Grad-CAM raise an interesting question: to what extent could FID be improved by merely nudging the generator to produce images that get classified to the same ImageNet classes as the real data? As we are interested in a potential weakness in FID, we furthermore want this nudging to happen so that the generated results do *not* actually improve in any real sense. In our terminology, operations that change FID without changing the generated results in a perceptible way are exploiting the *perceptual null space* of FID.

As our first attempt in Section 3.1, we will test a simple Top-1 (ImageNet classification) histogram matching between real and generated data. As this fails to reduce FID as much as we would like, we then develop a more general distribution resampling method in Section 3.2 and apply it to aligning Top-*N* histograms in Section 3.3. This approach manages to reduce FID very significantly, indicating that there exists a large perceptual null space in FID. Finally, in Section 4, we verify experimentally that this theoretical weakness also has practical relevance.

In our experiments, we use StyleGAN2 config-F trained in  $256 \times 256$  resolution without adaptive discriminator augmentation (ADA). The only exception is AFHQ-v2 DOG, where we enable ADA and train in  $512 \times 512$  resolution.<sup>2</sup> A difference between our FIDs for StyleGAN2 and the ones reported by [21] is caused by the use of different training configurations.

#### 3.1 Top-1 histogram matching

Based on the Grad-CAM visualizations in Section 2, one might suspect that to achieve a low FID, it would be sufficient to match the Top-1 class histograms between the sets of real and generated images. We tested this hypothesis by computing the Top-1 histogram for 50k real images, and then sampling an equal number of unique generated images for each Top-1 class. This was done by looking at the class probabilities at the output of the Inception-V3 classifier (Figure 1), and discarding the generated images that fall into a bin that is already full. Obtaining a perfect histogram match required drawing 800k–1.5M samples, depending on the dataset, with FFHQ being the fastest and LSUN PLACES taking the longest. Over multiple datasets, this simple Top-1 histogram matching consistently improves FID, by  $\sim 10\%$  (Table 1).

Does this mean that the set of generated images actually improved? Based on extensive visual inspection of the images, we are inclined to believe that the answer is likely “no”. (The supplement includes uncurated grids.) To answer this quantitatively, we compute a second pair of FIDs in the

<sup>2</sup>We use the official code <https://github.com/NVlabs/stylegan2-ada-pytorch>.

Table 2: Results of matching all fringe features. We compare the FID of randomly sampled images (FID) against ones that have been resampled to approximately match all fringe features with the training data (FID<sup>PL</sup>). The numbers represent averages over ten FID evaluations. Additionally, we report the corresponding numbers by replacing the Inception-V3 feature space with CLIP features (FID<sub>CLIP</sub>, FID<sub>CLIP</sub><sup>PL</sup>). Note that we use CLIP only when computing FID; the resampling is still done using Inception-V3. The numerical values of FID and FID<sub>CLIP</sub> are not comparable. The gray column (FID<sup>L</sup>) shows an additional experiment where the resampling is done using logits instead of pre-logits.

Dataset	FID	FID <sup>PL</sup>	FID <sup>L</sup>	FID <sub>CLIP</sub>	FID <sub>CLIP</sub> <sup>PL</sup>
FFHQ	5.63	1.82 (-67.7%)	2.31 (-59.0%)	2.90	2.78 (-4.1%)
LSUN CAT	8.35	3.05 (-63.5%)	3.88 (-53.5%)	8.95	7.98 (-10.8%)
LSUN CAR	5.75	2.11 (-63.3%)	2.59 (-55.0%)	7.76	7.33 (-5.5%)
LSUN PLACES	13.05	3.59 (-72.5%)	4.43 (-66.1%)	16.36	14.54 (-11.1%)
AFHQ-V2 DOG	10.58	5.92 (-44.0%)	6.27 (-40.7%)	4.23	4.04 (-4.5%)

image embedding space of CLIP (FID<sub>CLIP</sub>) [43].<sup>3</sup> CLIP’s features can be expected to be just as good for distance computations, and crucially, they should have little overlap with Inception features because CLIP was trained using different data and the different task of matching images with captions. A genuine improvement in the generated image distribution should be clearly visible in both FIDs. Yet, we can see that while FID<sub>CLIP</sub> is slightly affected, the improvement is an order of magnitude lower. This underlines the fact that histogram matching is an attack against (Inception-V3) FID and the improvement lies in the perceptual null space, i.e., it is not actually visible in the generated images.

### 3.2 Matching all fringe features

The previous experiment shows that merely matching Top-1 class histograms between real and generated images improves FID by exploiting the perceptual null space, but we want to go further. Extending the simple “draw samples until it falls into the right bin”-approach to Top- $N$  histogram matching would be computationally infeasible. We will now design a general technique for resampling the distribution of generated images, with the goal of approximately matching *all* fringe features. In the next section we will modify this approach to do Top- $N$  histogram matching.

Our idea is to first generate a larger set of candidate images ( $5\times$  oversampling), and then carefully select a subset of these candidates so that FID decreases. We approach this by directly optimizing FID as follows. First, we select a *candidate set* of 250k generated images and compute their Inception-V3 features. We then assign a non-negative scalar weight  $w_i$  to each generated image, and continuously optimize them to minimize the FID computed from *weighted* means and covariances of the generated images. When the optimization is finished, we use the weights as sampling probabilities and draw 50k random samples with replacement from the set of 250k candidate images.

More precisely, we optimize

$$\min_{\mathbf{w}} \left( \|\boldsymbol{\mu}_r - \boldsymbol{\mu}_g(\mathbf{w})\|_2^2 + \text{Tr} \left( \boldsymbol{\Sigma}_r + \boldsymbol{\Sigma}_g(\mathbf{w}) - 2(\boldsymbol{\Sigma}_r \boldsymbol{\Sigma}_g(\mathbf{w}))^{\frac{1}{2}} \right) \right), \quad (3)$$

where  $\boldsymbol{\mu}_g(\mathbf{w}) = \frac{\sum_i w_i \mathbf{f}_i}{\sum_i w_i}$  and  $\boldsymbol{\Sigma}_g(\mathbf{w}) = \frac{1}{\sum_i w_i} \sum_i w_i (\mathbf{f}_i - \boldsymbol{\mu}_g(\mathbf{w}))^T (\mathbf{f}_i - \boldsymbol{\mu}_g(\mathbf{w}))$  are the weighted mean and covariance of generated features  $\mathbf{f}_i$ , respectively. In practice, we optimize the weights in Equation 3 via gradient descent. We parameterize the weights as  $\log(w_i)$  to avoid negative values and facilitate easy conversion to probabilities. Note that we do not optimize the parameters of the generator network, only the sampling weights that are assigned to each generated image. Optimizing FID directly in this way is a form of adversarial attack, but not nearly as strong as the traditional way of modifying the images or the generator to directly attack the Inception-V3 network. In any case, our goal is only to elucidate the perceptual null space in FID, and we do not advocate this resampling step to improve the quality of models [19, 20].

Table 2 shows that FIDs can be drastically reduced using this approach. An improvement of this magnitude would be considered a major breakthrough in generative modeling — if it was real.

<sup>3</sup>We use the ViT-B/32 model available in <https://github.com/openai/CLIP>.

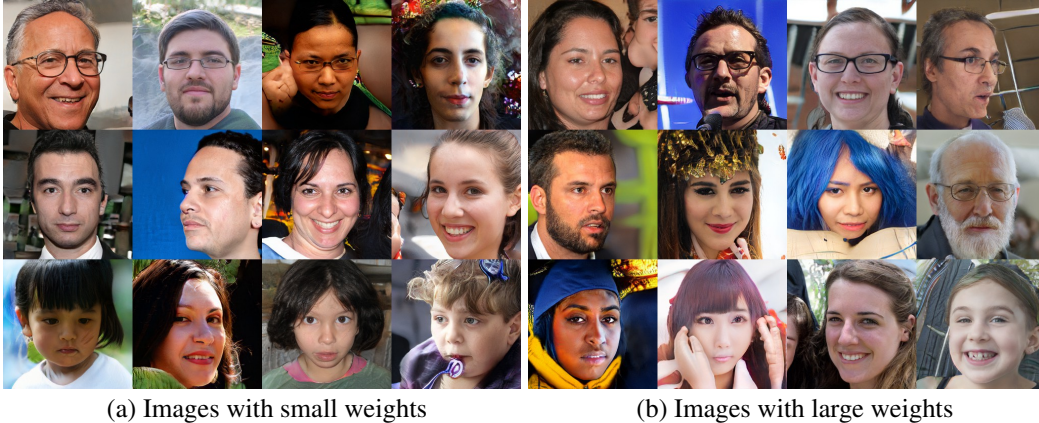


Figure 5: Uncurated random StyleGAN2 samples from images with (a) the smallest 10% of weights and (b) the largest 10% of weights after optimizing the weights to improve FID in the pre-logits space (Section 3.2). Both sets contain both realistic images and images with clear visual artifacts in apparently equal proportions, indicating that the large improvement in FID cannot be attributed to resampling simply assigning a lower weight to unrealistic images. The reader is encouraged to zoom in electronically. See supplementary material for a larger sample.

Figure 5 shows images that obtain small and large weights in the optimization; it is not at all clear that there is a visual difference between the sets. In particular, the resampling step does not reliably remove images with clear artifacts. The supplementary material includes larger sets of resampled and randomly generated images, along with numerical results showing that the resampling fools KID just as thoroughly as FID, even though we do not directly optimize KID.

To confirm the visual result quantitatively, we again compute  $FID_{CLIP}$  on the resampled distributions and observe that this “second opinion” indicates an order of magnitude lower improvement. This leads us to conclude that almost all of the improvement in FID is actually in the perceptual null space, and that this null space is therefore quite large. In other words, FID can be manipulated to a great extent through the ImageNet classification probabilities, without actually improving the generated results.

We can furthermore see that it makes only a small difference whether the weight optimization is carried out in the typical pre-logit space (denoted  $FID^{PL}$ ) or in the logit space ( $FID^L$ ), confirming that these spaces encode approximately the same information. Figure 1 illustrates the difference between these spaces.

### 3.3 Top- $N$ histogram matching

The drastic FID reduction observed in the previous section is clearly a result of an adversarial attack, but it does provide clues about the upper bound of the size of the perceptual null space. We will now further explore the nature of this null space by extending our resampling method to approximate Top- $N$  histogram matching. Then, by sweeping over  $N$ , we can gain further insights to how important the top classification results are for FID.

We implement this by carrying out the weight optimization in the space of class probabilities (see Figure 1). We furthermore binarize the class probability vectors by identifying the  $N$  classes with the highest probabilities and setting the corresponding entries to 1 and the rest to 0. These vectors now indicate, for each image, the Top- $N$  classes, while discarding their estimated probabilities. By matching the statistics of these indicator vectors between real and generated distributions, we optimize the co-occurrence of Top- $N$  classes. The result of the weight optimization is therefore an approximation of Top- $N$  histogram matching. With  $N = 1$ , the results approximately align with simple histogram matching (Section 3.1, Table 1). Note that the binarization is done before the weight optimization begins, and thus we don’t need its (non-computable) gradients.

Figure 6 shows how FID (computed in the usual pre-logit space) changes as we optimize Top- $N$  histogram matching with increasing  $N$ . We observe that even with small values of  $N$ , FID improves

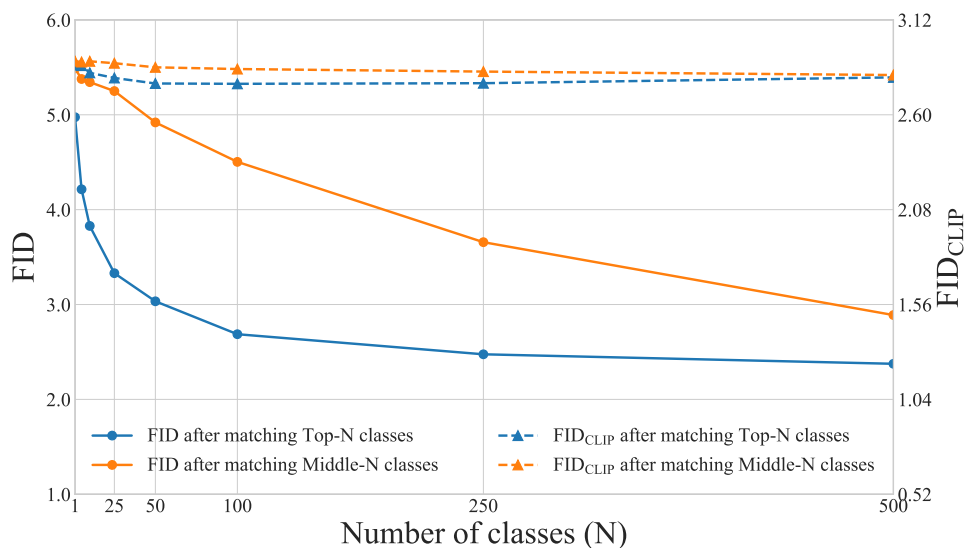


Figure 6: Softly matching Top- $N$  class distributions in FFHQ through resampling (Section 3.3). FID (solid curves, left-hand  $y$  scale) decreases sharply with increasing number  $N$  of classes included in the Top- $N$  indicator vectors, with  $N = 10$  already yielding a highly significant improvement over the unoptimized model. At the same time,  $FID_{CLIP}$  (dashed curves, right-hand  $y$  scale) remains almost constant, indicating that the apparent improvements in FID are superfluous. The orange control curves have been computed from classes in the middle of the sorted probability vectors, indicating that the top classes indeed have a much stronger influence. As the numerical values of FID and  $FID_{CLIP}$  are not comparable, the left and right  $y$  axes have been normalized so that the unoptimized results are at the same height, and zero — would it be visible on the axes — would be on the same height. This ensures relative changes are represented accurately.

rapidly, and converges to a value slightly higher than was obtained by optimizing the weights in the pre-logit space ( $FID^{PL}$  in Table 2). This demonstrates that FID is, to a significant degree, determined by the co-occurrence of top ImageNet classes. Furthermore, it illustrates that FID is the most interested in a handful of features whose only purpose is to help with ImageNet classification, not on some careful analysis of the whole image. As a further validation of this tendency, we also computed a similar optimization using binarized vectors computed using  $N$  classes chosen from the *middle*<sup>4</sup> of the sorted probabilities (orange curves in Figure 6). The results show that the top classes have a significantly higher influence on FID than those ranked lower by an Inception-V3 classifier. Finally, as before, we present a control  $FID_{CLIP}$  (dashed curves) that shows that CLIP’s feature space is indifferent to the apparent FID improvements yielded by the better alignment of Top- $N$  ImageNet classes. Though we only present results for FFHQ here, qualitative behavior is similar for LSUN CAT/PLACES/CAR, and AFHQ-v2 DOG.

These results indicate that it is certainly possible that some models receive an unrealistically low FID simply because they happen to reproduce the (inconsequential) ImageNet class distribution detected in the training data. Perhaps the most obvious way this could happen in practice is when ImageNet pre-training has been used for the discriminator, and the discriminator is therefore readily sensitive to the ImageNet features, which it may guide the generator to replicate. We will now investigate a real example where this seems to have happened.

<sup>4</sup>Our binarization methodology works only when  $\leq 50\%$  of classes are set to 1. After that the roles of 0 and 1 flip and the FID curves repeat themselves symmetrically. That’s why we used middle entries instead of the lowest entries.

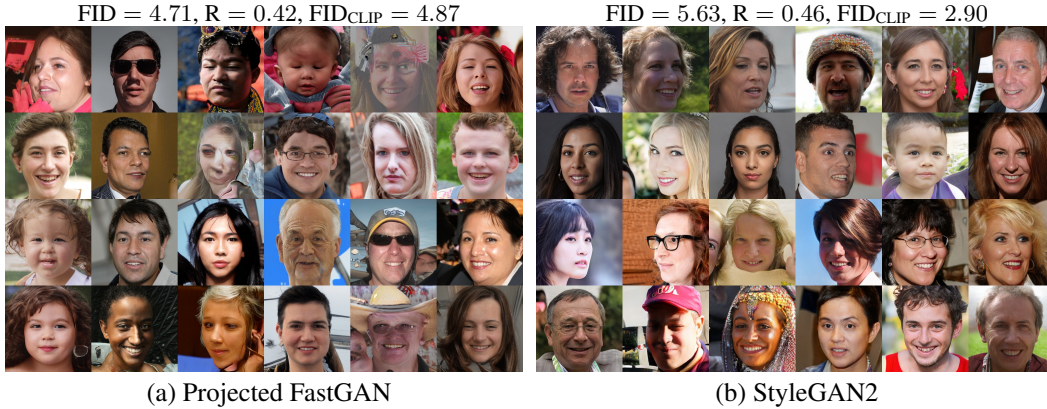


Figure 7: Uncurated samples from (a) Projected FastGAN and (b) StyleGAN2. While Projected FastGAN achieves a better FID, the samples contain clearly more artifacts. In contrast, Projected FastGAN has significantly higher FID<sub>CLIP</sub>, consistent with the observed quality differential. This implies that the pre-trained features employed by Projected FastGAN have unintentional interference with (Inception-V3) FID.

#### 4 An example of practical relevance

Recently, the use of ImageNet pre-trained classifiers as feature extractors for the discriminator network has received attention in GAN training [28, 49]. This has been observed to lead to much faster convergence and significant improvements in FID. We will now test whether some of these improvements might be in the perceptual nullspace of FID, i.e., not actually visible in the generated results.

We study this in the same context as Sauer et al. [49] by training a Projected FastGAN [31, 49], which uses an ImageNet pre-trained EfficientNet [55] as a feature extractor of the discriminator, and compare it against StyleGAN2 in FFHQ.<sup>5</sup>

The human preference study conducted by Sauer et al. [49] concludes that despite the dramatic improvements in FID, Projected FastGAN tends to generate lower quality and less diverse FFHQ samples than StyleGAN2. We verify this by comparing samples from Projected FastGAN and StyleGAN2 in a setup where FIDs are roughly comparable and the models reproduce a similar degree of variation as measured by recall (R) [29]. Visual inspection of uncurated samples (Figure 7) indeed reveals that Projected FastGAN produces much more distortions in the human faces than StyleGAN2 (see supplementary for larger image grids).

In this iso-FID comparison, FID<sub>CLIP</sub> agrees with human assessment – StyleGAN2 is rated significantly better than Projected FastGAN. It therefore seems clear that Projected FastGAN has lower FID than it should have, confirming that at least some of its apparent improvements are in the perceptual null space. We believe that the reason for this is the accidental leak of information from the pre-trained network, causing the model to replicate the ImageNet-like aspects in the training data more keenly. This observation does not mean that ImageNet pre-training is a bad idea, but it does mean that such pre-training can make FID unreliable in practice.

We also suspect that similar interference with FID can happen when the ImageNet pre-trained classifiers are used to curate the training data [9] or as a part of the sampling process [57].

#### 5 Conclusions

The numerical values of FID have a number of important uses. Large values indicate training failures quite reliably, and FID appears highly dependable when monitoring the convergence of a training run. FID improvements obtained through hyperparameter sweeps or other trivial changes generally

<sup>5</sup>We use the official code [https://github.com/autonomousvision/projected\\_gan](https://github.com/autonomousvision/projected_gan) with default hyperparameters.

seem to translate to better (subjective) results, even when the distributions are well aligned.<sup>6</sup> The caveats arise when two sufficiently different architectures and/or training setups are compared. If one of them is, for some reason, inclined to better reproduce the fringe features, it can lead to a much lower FIDs without a corresponding improvement in the human-observable quality.

Particular care should be exercised when introducing ImageNet pre-training to generative models [28, 49, 50]. This can be beneficial because a pre-trained discriminator can immediately focus on salient features, but as we have demonstrated, it can also compromise the validity of FID as a quality metric. This effect is particularly difficult to quantify because all other metrics currently in widespread use (KID and Precision/Recall) also rely on the feature spaces of ImageNet classifiers. To avoid this pitfall, it would be advisable to pre-train the discriminator using a task unrelated to ImageNet classification. As a partial solution, the FID improvements should at least be verified using a non-ImageNet trained (and thus non-standard) Fréchet distance. Viable alternative feature spaces include CLIP [43], which we used, and self-supervised SwAV classifier [5, 33]. An uninitialized network may also be a possibility [34, 50]. However, the properties of these feature spaces as a basis for FID should be critically examined in future work.

## References

- [1] Abadi, M., Agarwal, A., Barham, P., Brevdo, E., Chen, Z., Citro, C., Corrado, G.S., Davis, A., Dean, J., Devin, M., Ghemawat, S., Goodfellow, I., Harp, A., Irving, G., Isard, M., Jia, Y., Jozefowicz, R., Kaiser, L., Kudlur, M., Levenberg, J., Mané, D., Monga, R., Moore, S., Murray, D., Olah, C., Schuster, M., Shlens, J., Steiner, B., Sutskever, I., Talwar, K., Tucker, P., Vanhoucke, V., Vasudevan, V., Viégas, F., Vinyals, O., Warden, P., Wattenberg, M., Wicke, M., Yu, Y., Zheng, X.: *TensorFlow: Large-Scale Machine Learning on Heterogeneous Systems* (2015), <https://www.tensorflow.org/>
- [2] Bell-Kligler, S., Shocher, A., Irani, M.: *Blind Super-Resolution Kernel Estimation using an Internal-GAN*. In: *Proc. NeurIPS* (2019)
- [3] Binkowski, M., Sutherland, D.J., Arbel, M., Gretton, A.: *Demystifying MMD GANs*. In: *Proc. ICLR* (2018)
- [4] Brock, A., Donahue, J., Simonyan, K.: *Large Scale GAN Training for High Fidelity Natural Image Synthesis*. In: *Proc. ICLR* (2019)
- [5] Caron, M., Misra, I., Mairal, J., Goyal, P., Bojanowski, P., Joulin, A.: *Unsupervised Learning of Visual Features by Contrasting Cluster Assignments*. In: *Proc. NeurIPS* (2020)
- [6] Choi, Y., Uh, Y., Yoo, J., Ha, J.W.: *StarGAN v2: Diverse Image Synthesis for Multiple Domains*. In: *Proc. CVPR* (2020)
- [7] Chong, M.J., Forsyth, D.: *Effectively Unbiased FID and Inception Score and Where to Find Them*. In: *Proc. CVPR* (2020)
- [8] Deng, J., Dong, W., Socher, R., Li, L.J., Li, K., Fei-Fei, L.: *ImageNet: A Large-Scale Hierarchical Image Database*. In: *Proc. CVPR* (2009)
- [9] DeVries, T., Drozdal, M., Taylor, G.W.: *Instance Selection for GANs*. In: *Proc. NeurIPS* (2020)
- [10] Dinh, L., Sohl-Dickstein, J., Bengio, S.: *Density Estimation using Real NVP*. In: *Proc. ICLR* (2017)
- [11] Dowson, D., Landau, B.: *The Fréchet distance between multivariate normal distributions*. *Journal of Multivariate Analysis* **12**, 450–455 (1982)
- [12] Esser, P., Rombach, R., Ommer, B.: *Taming Transformers for High-Resolution Image Synthesis*. In: *Proc. CVPR* (2021)
- [13] Geirhos, R., Rubisch, P., Michaelis, C., Bethge, M., Wichmann, F., Brendel, W.: *ImageNet-trained CNNs are biased towards texture; increasing shape bias improves accuracy and robustness*. In: *Proc. ICLR* (2019)
- [14] Goodfellow, I., Pouget-Abadie, J., Mirza, M., Xu, B., Warde-Farley, D., Ozair, S., Courville, A., Bengio, Y.: *Generative Adversarial Networks*. In: *Proc. NIPS* (2014)
- [15] Hermann, K.L., Chen, T., Kornblith, S.: *The Origins and Prevalence of Texture Bias in Convolutional Neural Networks*. In: *Proc. NeurIPS* (2020)
- [16] Heusel, M., Ramsauer, H., Unterthiner, T., Nessler, B., Hochreiter, S.: *GANs Trained by a Two Time-Scale Update Rule Converge to a Local Nash Equilibrium*. In: *Proc. NIPS* (2017)
- [17] Ho, J., Jain, A., Abbeel, P.: *Denosing Diffusion Probabilistic Models*. In: *Proc. NeurIPS* (2020)

---

<sup>6</sup>Based on personal communication with individuals who have trained over 10,000 generative models.

- [18] Huang, X., Mallya, A., Wang, T.C., Liu, M.Y.: Multimodal Conditional Image Synthesis with Product-of-Experts GANs. CoRR **abs/2112.05130** (2021)
- [19] Humayun, A.I., Balestrieri, R., Baraniuk, R.: MaGNET: Uniform Sampling from Deep Generative Network Manifolds Without Retraining. In: Proc. ICLR (2022)
- [20] Issenhuth, T., Tanielian, U., Picard, D., Mary, J.: Latent reweighting, an almost free improvement for GANs. In: Proc. WACV (2022)
- [21] Karras, T., Aittala, M., Hellsten, J., Laine, S., Lehtinen, J., Aila, T.: Training Generative Adversarial Networks with Limited Data. In: Proc. NeurIPS (2020)
- [22] Karras, T., Aittala, M., Laine, S., Härkönen, E., Hellsten, J., Lehtinen, J., Aila, T.: Alias-Free Generative Adversarial Networks. In: Proc. NeurIPS (2021)
- [23] Karras, T., Laine, S., Aila, T.: A Style-Based Generator Architecture for Generative Adversarial Networks. In: Proc. CVPR (2019)
- [24] Karras, T., Laine, S., Aittala, M., Hellsten, J., Lehtinen, J., Aila, T.: Analyzing and Improving the Image Quality of StyleGAN. In: Proc. CVPR (2020)
- [25] Kim, J., Kim, M., Kang, H., Lee, K.: U-GAT-IT: Unsupervised Generative Attentional Networks with Adaptive Layer-Instance Normalization for Image-to-Image Translation. In: Proc. ICLR (2020)
- [26] Kingma, D.P., Dhariwal, P.: Glow: Generative Flow with Invertible 1x1 Convolutions. In: Proc. NeurIPS (2018)
- [27] Kingma, D.P., Welling, M.: Auto-Encoding Variational Bayes. In: Proc. ICLR (2014)
- [28] Kumari, N., Zhang, R., Shechtman, E., Zhu, J.Y.: Ensembling Off-the-shelf Models for GAN Training. CoRR **abs/2112.09130** (2021)
- [29] Kynkäänniemi, T., Karras, T., Laine, S., Lehtinen, J., Aila, T.: Improved Precision and Recall Metric for Assessing Generative Models. In: Proc. NeurIPS (2019)
- [30] Ledig, C., Theis, L., Huszár, F., Caballero, J., Aitken, A.P., Tejani, A., Totz, J., Wang, Z., Shi, W.: Photo-Realistic Single Image Super-Resolution Using a Generative Adversarial Network. In: Proc. CVPR (2017)
- [31] Liu, B., Zhu, Y., Song, K., Elgammal, A.: Towards Faster and Stabilized GAN Training for High-fidelity Few-shot Image Synthesis. In: Proc. ICLR (2021)
- [32] Lucic, M., Kurach, K., Michalski, M., Gelly, S., Bousquet, O.: Are GANs Created Equal? A Large-Scale Study. In: Proc. NeurIPS (2018)
- [33] Morozov, S., Voynov, A., Babenko, A.: On Self-Supervised Image Representations for GAN Evaluation. In: Proc. ICLR (2021)
- [34] Naeem, M.F., Oh, S.J., Uh, Y., Choi, Y., Yoo, J.: Reliable Fidelity and Diversity Metrics for Generative Models. In: Proc. ICML (2020)
- [35] Nichol, A., Dhariwal, P., Ramesh, A., Shyam, P., Mishkin, P., McGrew, B., Sutskever, I., Chen, M.: GLIDE: Towards Photorealistic Image Generation and Editing with Text-Guided Diffusion Models. CoRR **abs/2112.10741** (2021)
- [36] van den Oord, A., Kalchbrenner, N., Kavukcuoglu, K.: Pixel Recurrent Neural Networks. In: Proc. ICML (2016)
- [37] van den Oord, A., Kalchbrenner, N., Vinyals, O., Espeholt, L., Graves, A., Kavukcuoglu, K.: Conditional Image Generation with PixelCNN Decoders. In: Proc. NIPS (2016)
- [38] Park, T., Liu, M.Y., Wang, T., Zhu, J.Y.: Semantic Image Synthesis With Spatially-Adaptive Normalization. In: Proc. CVPR (2019)
- [39] Park, T., Zhu, J.Y., Wang, O., Lu, J., Shechtman, E., Efros, A.A., Zhang, R.: Swapping Autoencoder for Deep Image Manipulation. In: Proc. NeurIPS (2020)
- [40] Parmar, G., Zhang, R., Zhu, J.Y.: On Aliased Resizing and Surprising Subtleties in GAN Evaluation. CoRR **abs/2104.11222** (2021)
- [41] Paszke, A., Gross, S., Massa, F., Lerer, A., Bradbury, J., Chanan, G., Killeen, T., Lin, Z., Gimelshein, N., Antiga, L., Desmaison, A., Kopf, A., Yang, E., DeVito, Z., Raison, M., Tejani, A., Chilamkurthy, S., Steiner, B., Fang, L., Bai, J., Chintala, S.: PyTorch: An Imperative Style, High-Performance Deep Learning Library. In: Proc. NeurIPS (2019)
- [42] Pebay, P.P.: Formulas for robust, one-pass parallel computation of covariances and arbitrary-order statistical moments. Tech. Rep. SAND2008-6212, Sandia National Laboratories (2008)
- [43] Radford, A., Kim, J.W., Hallacy, C., Ramesh, A., Goh, G., Agarwal, S., Sastry, G., Askell, A., Mishkin, P., Clark, J., Krueger, G., Sutskever, I.: Learning Transferable Visual Models From Natural Language Supervision. In: Proc. ICML (2021)

- [44] Ramesh, A., Pavlov, M., Goh, G., Gray, S., Voss, C., Radford, A., Chen, M., Sutskever, I.: Zero-Shot Text-to-Image Generation. In: Proc. ICML (2021)
- [45] Razavi, A., van den Oord, A., Vinyals, O.: Generating Diverse High-Fidelity Images with VQ-VAE-2. In: Proc. NeurIPS (2019)
- [46] Saharia, C., Ho, J., Chan, W., Salimans, T., Fleet, D.J., Norouzi, M.: Image super-resolution via iterative refinement. arXiv preprint arXiv:2104.07636 (2021)
- [47] Sajjadi, M.S.M., Bachem, O., Lucic, M., Bousquet, O., Gelly, S.: Assessing Generative Models via Precision and Recall. In: Proc. NeurIPS (2018)
- [48] Salimans, T., Goodfellow, I., Zaremba, W., Cheung, V., Radford, A., Chen, X.: Improved Techniques for Training GANs. In: Proc. NIPS (2016)
- [49] Sauer, A., Chitta, K., Müller, J., Geiger, A.: Projected GANs Converge Faster. In: In Proc. NeurIPS (2021)
- [50] Sauer, A., Schwarz, K., Geiger, A.: StyleGAN-XL: Scaling StyleGAN to Large Diverse Datasets. CoRR **abs/2202.00273** (2022)
- [51] Selvaraju, R.R., Das, A., Vedantam, R., Cogswell, M., Parikh, D., Batra, D.: Grad-CAM: Visual Explanations from Deep Networks via Gradient-Based Localization. In: Proc. ICCV (2017)
- [52] Sohl-Dickstein, J., Weiss, E.A., Maheswaranathan, N., Ganguli, S.: Deep Unsupervised Learning using Nonequilibrium Thermodynamics. In: Proc. ICML (2015)
- [53] Song, Y., Ermon, S.: Generative Modeling by Estimating Gradients of the Data Distribution. In: Proc. NeurIPS (2019)
- [54] Szegedy, C., Vanhoucke, V., Ioffe, S., Shlens, J., Wojna, Z.: Rethinking the Inception Architecture for Computer Vision. In: Proc. CVPR (2016)
- [55] Tan, M., Le, Q.V.: EfficientNet: Rethinking Model Scaling for Convolutional Neural Networks. In: Proc. ICML (2019)
- [56] van Steenkiste, S., Kurach, K., Schmidhuber, J., Gelly, S.: Investigating object compositionality in Generative Adversarial Networks. Neural Networks (2020)
- [57] Watson, D., Chan, W., Ho, J., Norouzi, M.: Learning Fast Samplers for Diffusion Models by Differentiating Through Sample Quality. In: Proc. ICLR (2022)
- [58] Xu, Q., Huang, G., Yuan, Y., Guo, C., Sun, Y., Wu, F., Weinberger, K.Q.: An Empirical Study on Evaluation Metrics of Generative Adversarial Networks. ArXiv **abs/1806.07755** (2018)
- [59] Yu, F., Seff, A., Zhang, Y., Song, S., Funkhouser, T., Xiao, J.: LSUN: Construction of a Large-scale Image Dataset using Deep Learning with Humans in the Loop. CoRR **abs/1506.03365** (2015)
- [60] Zhang, R., Isola, P., Efros, A.A., Shechtman, E., Wang, O.: The Unreasonable Effectiveness of Deep Features as a Perceptual Metric. In: Proc. CVPR (2018)
- [61] Zhou, S., Gordon, M.L., Krishna, R., Narcomey, A., Fei-Fei, L., Bernstein, M.S.: HYPE: A Benchmark for Human eYe Perceptual Evaluation of Generative Models. In: Proc. NeurIPS (2019)
- [62] Zhu, J.Y., Park, T., Isola, P., Efros, A.A.: Unpaired Image-to-Image Translation using Cycle-Consistent Adversarial Networks. In: Proc. ICCV (2017)

Sample size	FFHQ	LSUN Cat
5k + 5k	8.91 $\pm$ 0.15	13.01 $\pm$ 0.14
10k + 10k	6.98 $\pm$ 0.02	10.33 $\pm$ 0.10
50k + 50k	5.63 $\pm$ 0.03	8.35 $\pm$ 0.03
All + 50k	5.41 $\pm$ 0.05	7.86 $\pm$ 0.04

(a) Number of samples

	FFHQ	LSUN Cat
TensorFlow	5.63 $\pm$ 0.05	8.35 $\pm$ 0.03
PyTorch	3.92 $\pm$ 0.04	6.69 $\pm$ 0.03

(b) Inception-V3 instance

Figure 8: FID is very sensitive to (a) the number samples (real + generated) and (b) the exact instance of the Inception-V3 network. The tables report the mean  $\pm$  standard deviation of FID for a given StyleGAN2 generator over ten evaluations with different random seeds.

## A Related work in understanding FID

Previous work has uncovered various details that have a surprisingly large effect on the exact value of FID [3, 7, 32, 40]. These observations are important to acknowledge because reproducing results from comparison methods is not always possible and one might be forced to resort to copying the reported FID results. In that case, even small differences in the FID evaluation protocol might cause erroneous rankings between models.

**Number of samples and bias.** FID depends strongly on the number of samples used in evaluation (Figure 8a). Therefore it is crucial to standardize to a specific number of real and generated samples [3]. Furthermore, Binkowski et al. [3] and Chong and Forsyth [7] note that the estimator of FID is biased and additionally, that there exists no unbiased estimator of FID. Consequently, using an insufficient amount of samples in evaluation can lead to inconsistent ranking between models because the bias in FID is not constant between models [7].

**Network architecture.** FID is also very sensitive to the chosen feature network instance or type. Many deep learning frameworks (e.g. PyTorch [41], Tensorflow [1]) provide their own versions of the Inception-V3 network with distinct weights. Figure 8b shows that FID is surprisingly sensitive to the exact instance of the Inception-V3 network. The discrepancies are certainly large enough to confuse with state-of-the-art performance. In practice, the official Tensorflow network must be used for comparable results.<sup>7</sup>

Lucic et al. [32] reported that the *ranking* of models with FID is not sensitive to the selected network architecture – it only has an effect on the absolute value range of FIDs, but the relative ordering of the models remains approximately the same. However, our tests with FID<sub>CLIP</sub> indicate that this observation likely holds only between different ImageNet classifier networks.

**Image processing flaws.** Before feeding images to the Inception-V3, they need to be resized to  $299 \times 299$  resolution. Parmar et al. [40] noted that the image resize functions of the most commonly used deep learning libraries [1, 41] introduce aliasing artifacts due to poor pre-filtering. They demonstrate that this aliasing has a noticeable effect on FID.

<sup>7</sup><http://download.tensorflow.org/models/image/imagenet/inception-2015-12-05.tgz>

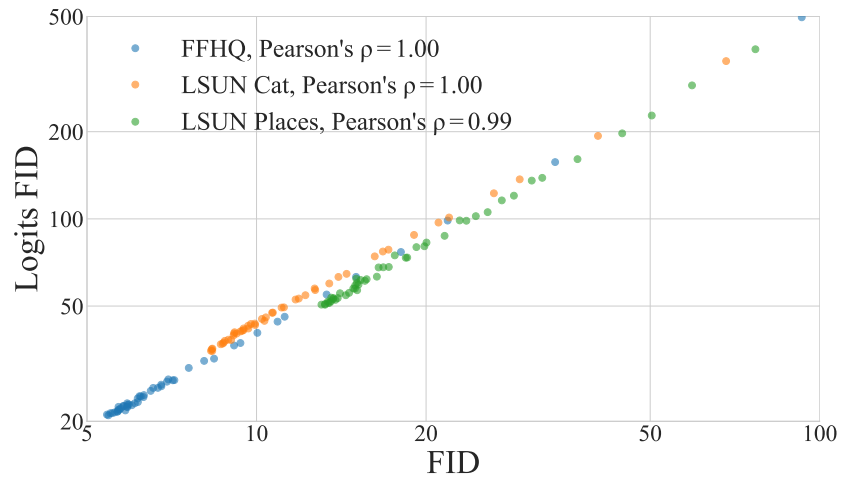


Figure 9: We observe nearly perfect correlation between FIDs computed from pre-logit features and classification logits since these two are separated by only one affine transformation. Each point corresponds to a single StyleGAN2 training snapshot in  $256 \times 256$  resolution.

## B Correlation between pre-logits and logits FID

Figure 9 demonstrates that FIDs calculated from the pre-logits and logits are highly correlated. The high correlation is explained by the fact that these two spaces are separated by only one affine transformation and without any non-linearities. Note that this test is only a guiding experiment to help find out to what FID is sensitive to and it is not guaranteed to hold for different GAN architectures or training setups.

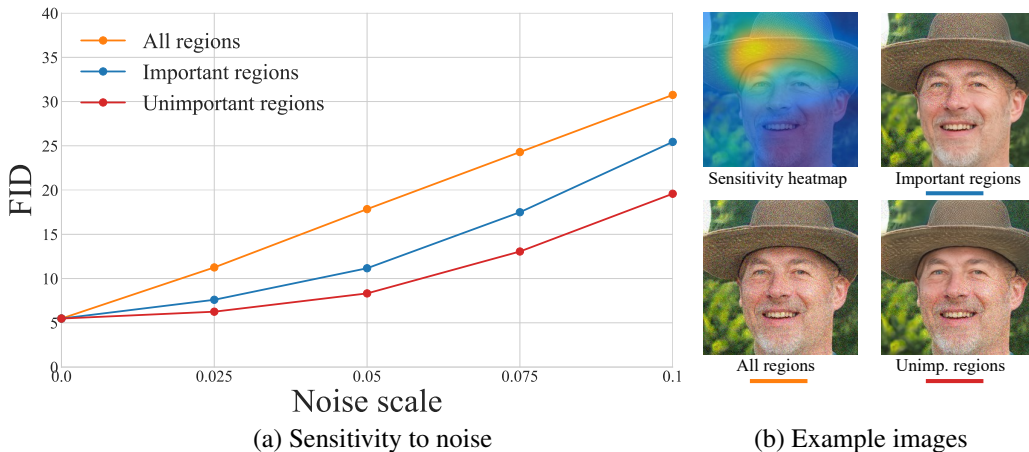


Figure 10: (a) Adding Gaussian noise to regions that are important for FID (blue curve) leads to the larger increase compared to adding noise in unimportant regions. (b) Image showing regions FID considers as the most important and noise added to different regions at scale 0.05. We recommend zooming in (b) to better assess the noise.

## C What does FID look at in an image?

**Validation of FID sensitivity heatmaps.** To validate how reliably our sensitivity heatmaps highlight the most important regions for FID, we perform an additional experiment where we add Gaussian noise to either important or unimportant areas, while keeping the other clean without noise. To cancel out effects that may arise from adding different amounts of noise, measured in pixel area, we divide the pixels of the images equally between the important and unimportant regions.

Figure 10a shows FID when we add an increasing amount of Gaussian noise to different regions of the images and Figure 10b demonstrates the appearance of the noisy images. Adding noise everywhere in the image is an upper bound how greatly FID can increase in this test setup. Adding noise to the important regions leads to FID larger increase in FID, compared to adding noise to the unimportant regions.

**Additional FID sensitivity heatmaps.** Figure 11 presents more FID sensitivity heatmaps for individual StyleGAN2 generated images using FFHQ and LSUN CAT and their corresponding ImageNet Top-1 classifications in the top left corner. For both datasets the regions for which FID is the most sensitive to are highly localized and correlate strongly with the Top-1 class.

Figure 12 shows additional mean images and heatmaps for StyleGAN2 generated images for FFHQ that get classified to a certain class. On average FID is the most sensitive to the pixel locations where the Top-1 class is intuitively located and relatively insensitive to the human faces.



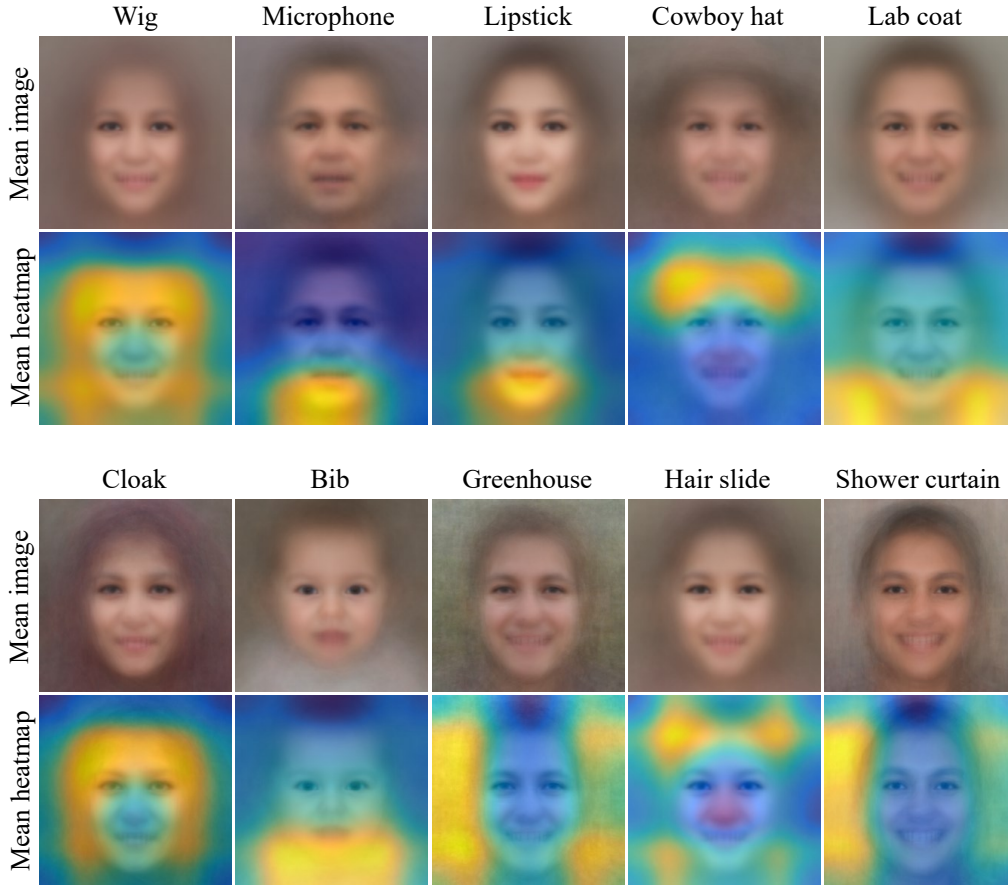


Figure 12: Mean images and heatmaps of regions that are the most important for FID with StyleGAN2 images in FFHQ that get classified to some class, e.g., “lipstick”. The heatmaps highlight the regions of Top-1 classes that are typically located outside the face area.

## D Probing the perceptual null space in FID

**Pseudocode and implementation details.** Algorithm 1 shows the pseudocode for our resampling method. Function OPTIMIZE-RESAMPLING-WEIGHTS optimizes the per-image sampling weights such that FID between real and weighted generated features is minimized. The inputs to the function are sets of features for real and generated images  $F_r$  and  $F_g$ , respectively, learning rate  $\alpha$  and maximum number of iterations  $T$ . Note that the features do not have to be the typical pre-logits features where standard FID is calculated, they can be, e.g., logits or binarized class probabilities. First, we calculate the statistics of real features (lines 3-4) and then initialize the per-image log-parameterized weights  $w_i$  to zeros (line 7). Then, for  $T$  iterations we calculate the weighted mean and covariance of generated features (lines 11-12) and update the weights via gradient descent to minimize FID (line 15). After optimization the log-parameterized weights can be transformed into sampling probabilities with  $p_i = \frac{e^{w_i}}{\sum_j e^{w_j}}$ , where  $p_i$  is the probability of sampling  $i$ th feature. We sample with replacement according to these probabilities to calculate our resampled FIDs ( $FID^{PL}$ ,  $FID^L$ ,  $FID_{CLIP}^{PL}$ ) with 50k real and generated features.

In practice, we use features of 50k real and 250k generated images for all datasets, except for AFHQ-v2 DOG where we use 4678 real and 25k generated images. We use learning rate  $\alpha = 10.0$  when optimizing pre-logits features and  $\alpha = 5.0$  when optimizing logits or binarized class probabilities. We optimize the weights until convergence, which typically requires  $\sim 100k$  iterations. We select the weights that lead to the smallest FID with 50k real and 50k generated features that are sampled according to the optimized weights. In the optimization, we do not apply exponential moving

---

**Algorithm 1** Resampling algorithm pseudocode.

---

```
1: function OPTIMIZE-RESAMPLING-WEIGHTS( $\mathbf{F}_r, \mathbf{F}_g, \alpha, T$ )
2:   Calculate feature statistics of reals.
3:    $\boldsymbol{\mu}_r \leftarrow \frac{1}{|\mathbf{F}_r|} \sum_i \mathbf{f}_r^i$ 
4:    $\boldsymbol{\Sigma}_r \leftarrow \frac{1}{|\mathbf{F}_r|-1} \sum_i (\mathbf{f}_r^i - \boldsymbol{\mu}_r)^T (\mathbf{f}_r^i - \boldsymbol{\mu}_r)$ 
5:
6:   Initialize log-parameterized per-image weights  $w$  to zeros.
7:    $w_i = 0, \forall i$ 
8:
9:   for  $T$  iterations do
10:    Compute weighted mean and covariance of generated features.
11:     $\boldsymbol{\mu}_g(w) \leftarrow \frac{\sum_i e^{w_i} \mathbf{f}_g^i}{\sum_i e^{w_i}}$ 
12:     $\boldsymbol{\Sigma}_g(w) \leftarrow \frac{1}{\sum_i e^{w_i}} \sum_i e^{w_i} (\mathbf{f}_g^i - \boldsymbol{\mu}_g(w))^T (\mathbf{f}_g^i - \boldsymbol{\mu}_g(w))$ 
13:
14:    Update the weights.
15:     $w \leftarrow w - \alpha \nabla_w \text{FID}(\boldsymbol{\mu}_r, \boldsymbol{\Sigma}_r, \boldsymbol{\mu}_g(w), \boldsymbol{\Sigma}_g(w))$ 
16:
17:   return  $w$ 
```

---

Table 3: Optimizing FID also decreases KID significantly. We compare the KID of randomly sampled images (KID) against KID that is calculated by resampling according to the weights obtained from optimizing FID in the pre-logits features (KID<sup>PL</sup>). The numbers are means over ten KID evaluations.

Dataset	FID	FID <sup>PL</sup>		KID $\times 10^3$	KID <sup>PL</sup> $\times 10^3$	
FFHQ	5.63	1.82	(-67.7%)	1.92	0.23	(-88.0%)
LSUN CAT	8.35	3.05	(-63.5%)	2.98	0.37	(-87.6%)
LSUN CAR	5.75	2.11	(-63.3%)	2.48	0.32	(-87.1%)
LSUN PLACES	13.05	3.59	(-72.5%)	7.36	0.31	(-95.8%)
AFHQ-v2 DOG	10.58	5.92	(-44.0%)	2.08	0.12	(-94.2%)

average to the weights or learning rate decay. We use 32GB NVIDIA Tesla V100 GPU to run our resampling experiments. One weight optimization run with 50k real and 250k generated features takes approximately 36h where most the execution time goes into calculating the matrix square root in FID with eigenvalue decomposition. We will make our code publicly available.

**Image grids for Top-1 matching and pre-logits resampling.** Figure 13 shows uncurated image grids when we sample StyleGAN2 generated images randomly, after Top-1 histogram matching, and after optimizing FID in the pre-logits feature space. Even though Top-1 histogram matching and pre-logits resampling reduce FID, the visual appearance of the generated images remains largely unchanged. FID<sub>CLIP</sub> values further demonstrate that the improvement in FID falls into the perceptual null space.

In Figure 14, we show more images that obtain a small or large weight after optimizing FID in the pre-logits feature space. A low FID after resampling can not be attributed to simply removing images with clear visual artifacts.

**Effect of pre-logits resampling on KID.** Table 3 shows that resampling in pre-logits feature space also strongly decreases Kernel Inception Distance (KID) [3], even though we do not explicitly optimize KID. This is because the both metrics are measured in the same feature space and therefore we hypothesize that they share approximately the same perceptual null space.

**Top- $N$  histogram matching.** We show further results from approximate Top- $N$  histogram matching in LSUN CAT/CAR/PLACES and AFHQ-v2 DOG in Figure 15. FID can be consistently improved by aligning the Top- $N$  histograms of real and generated images. Furthermore, the largest decrease in FID can be obtained by including information of the most probable classes.



(a) Random sample (FID = 5.63, FID<sub>CLIP</sub> = 2.90)



(b) Top-1 matching (FID = 4.91, FID<sub>CLIP</sub> = 2.86)

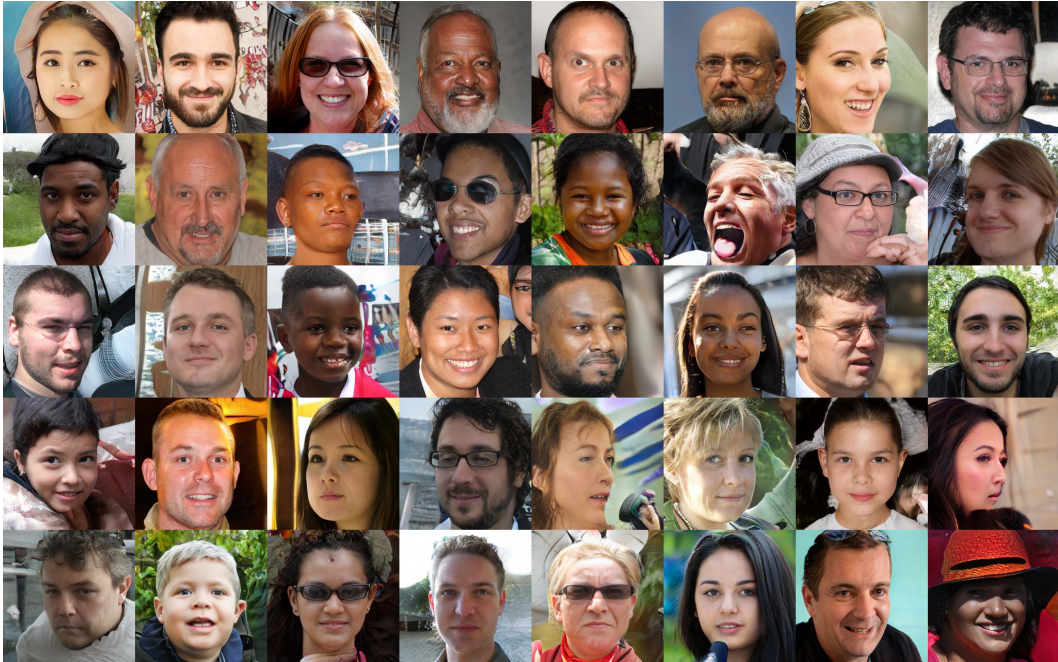


(c) Pre-logits resampling (FID = 1.82, FID<sub>CLIP</sub> = 2.78)

Figure 13: FID can be drastically reduced by using our resampling approach without improving the visual fidelity of the generated images. (a) Randomly sampled StyleGAN2 images, (b) randomly sampled StyleGAN2 images after Top-1 histogram matching, and (c) StyleGAN2 images sampled according to weights that were optimized in the pre-logits feature space.

## E An example of practical relevance

**Larger Projected FastGAN and StyleGAN2 image grids.** Figure 16 shows a larger image grid of StyleGAN2 and Projected FastGAN generated images for FFHQ. The models obtain similar FID but StyleGAN2 gets significantly lower FID<sub>CLIP</sub>. This implies that some of the FID improvement in Projected FastGAN happens in the perceptual null space because ImageNet pre-trained features are used as a part of the discriminator network.



(a) Images with small weights



(b) Images with large weights

Figure 14: Random StyleGAN2 images sampled among (a) the smallest 10% of weights and (b) the largest 10% of weights after optimizing the weights to minimize FID in the pre-logits space. Both sets contain realistic looking images and images with visual artifacts. Resampling in the pre-logits feature space does not remove all the images with visual artifacts.

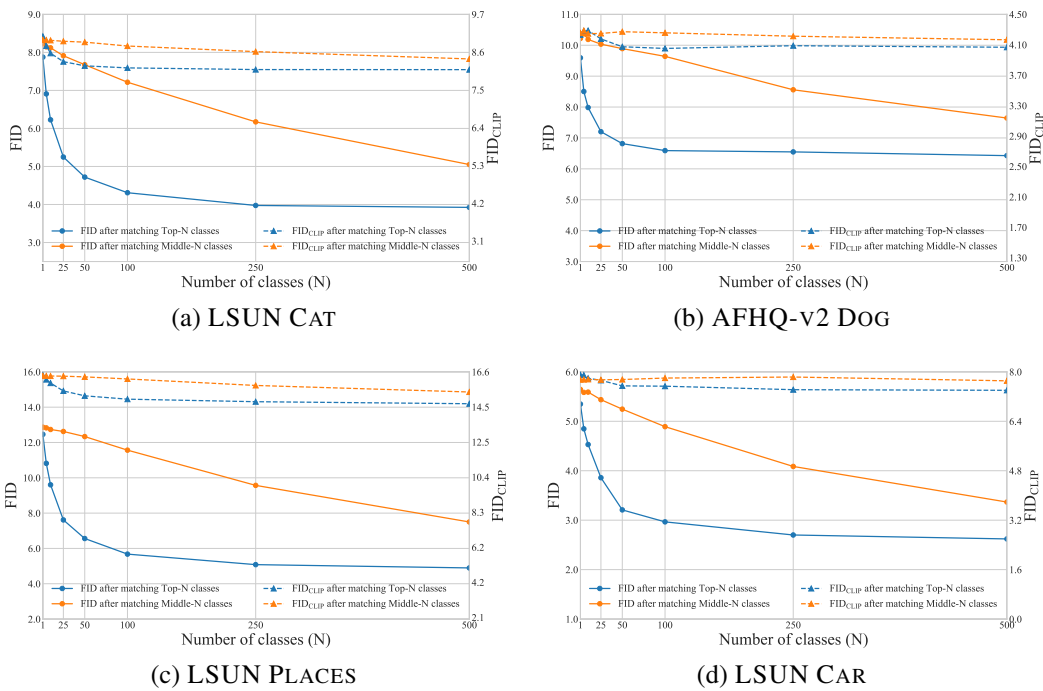


Figure 15: Additional results from aligning Top-N class histograms. For all datasets adding information from the Top-N ImageNet classes consistently leads to largest decrease in FID while FID<sub>CLIP</sub> remains almost unchanged.



(a) Projected FastGAN (FID = 4.71, R = 0.42, FID<sub>CLIP</sub> = 4.87)



(b) StyleGAN2 (FID = 5.63, R = 0.46, FID<sub>CLIP</sub> = 2.90)

Figure 16: Uncurated samples of (a) Projected FastGAN and (b) StyleGAN2 generated images. While Projected FastGAN achieves a better FID, the samples contain clearly more artifacts.